Engineering Structures 315 (2024) 118425

Contents lists available at ScienceDirect

Engineering Structures

journal homepage: www.elsevier.com/locate/engstruct

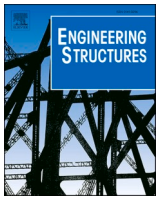

Experimental shear behaviour of masonry walls reinforced with FRCM

Valerio Alecci [a], Mario Fagone [b,*], Stefano Galassi [a], Tommaso Rotunno [a], Gianfranco Stipo [a], Mario De Stefano [a]

[a] Dipartimento di Architettura (DiDA), Università degli Studi di Firenze, Piazza Brunelleschi 6, 50121 Florence, Italy
[b] Dipartimento di Ingegneria Civile e Ambientale (DICEA), Università degli Studi di Firenze, via di S. Marta 3, 50139 Florence, Italy

ARTICLE INFO

Keywords:
Masonry panels
FRCM composite materials
Strengthening
Shear behaviour
Diagonal tests
Analytical assessment

ABSTRACT

The shear strength of piers and spandrels is a crucial factor in masonry buildings, affecting structural safety. Such a strength can be increased in several ways, particularly by using fiber reinforced cementitious matrix (FRCM) reinforcements. These reinforcements can be applied symmetrically on both sides of the wall or only on one side. As it is well known, the FRCM-to-substrate adhesive properties strongly affect the effectiveness of such reinforcements. Moreover, a complete covering of the reinforced surface with bidirectional mesh evenly distributes the stresses, improving the load-bearing capacity. Appropriate test methods, for example diagonal tests, can be effectively used to evaluate the shear capacity of masonry panels, even with externally bonded composite material reinforcements, and the corresponding failure mechanism. This paper describes the results of an experimental campaign involving masonry panels, made with three different types of mortar, also reinforced with a PBO-FRCM system, subjected to diagonal tests. Through the experimental results, it was possible to determine the shear capacity of the panels, identify the failure mechanisms and evaluate the effectiveness of the FRCM reinforcements. The predictive capability of design formulas proposed in the literature for evaluating the shear capacity of unreinforced and reinforced masonry panels has been analyzed in the paper.

1. Introduction

In masonry buildings, shear strength is an extremely important mechanical parameter as it can strongly influence the safety of the structure [1]. As it is well known, in fact, masonry piers and spandrels can be highly vulnerable to in-plane seismic actions [2,3], inducing shear stresses that cause the failure of such elements and activate the collapse mechanism. Therefore, the measurement and estimation of the actual shear capacity of these structural elements is a crucial aspect. This parameter depends on various factors, such as the geometry of the panels, the brickwork, the failure mode, the compressive stress generated by the vertical loads and, of course, the masonry shear strength. An estimate of the shear strength can be obtained by indirect or direct methods. Italian Building Code [4], in line with Eurocode 6 [5], allows to directly determine the shear strength of the masonry through two test methods: test on triplets [6] and diagonal tests [7–12]. The latter allows to determine the tensile strength of the masonry; then, the shear strength can be determined for example through the Turnesek-Cacovic criterion [13].

When the masonry shear capacity needs to be increased, the use of truly effective strengthening techniques becomes crucial for the preservation of historic masonry buildings belonging to the architectural heritage. The bonding of fibre-reinforced cement matrix (FRCM) reinforcements on masonry surfaces has proven to be a very effective technique for this purpose [14–35]. Such reinforcements, consisting of a fibre mesh (e.g. glass, PBO, etc.) embedded into an inorganic cementitious matrix, can be applied in different configurations. The best result is obtained by applying FRCM composites on both sides of the wall to achieve symmetrical reinforcement and maximize the overall effectiveness of the system; by doing so, an evenly distribution of the shear stresses over the structural element is achieved [36]. However, particular situations that could arise in interventions on existing buildings (for example the presence of fine finishes, frescoes, mosaics, etc. or the impossibility or inappropriateness to evacuate the building or interrupt its functions) and the application of today's historical heritage conservation criteria could suggest or oblige to apply the reinforcement only on one side of the wall to reduce its impact. In so doing, the effectiveness of the reinforcement decreases because of the introduced eccentricities in the wall behaviour. In some applications, the use of mechanical connections that improve the adhesive capacity of the reinforcement

* Corresponding author.
E-mail address: mario.fagone@unifi.it (M. Fagone).

https://doi.org/10.1016/j.engstruct.2024.118425
Received 5 March 2024; Received in revised form 15 May 2024; Accepted 9 June 2024
Available online 26 June 2024

and its effectiveness can also be considered. Note that the effects of any asymmetry of the reinforcement (possibly applied on only one face of the wall) are not explicitly considered in the design formulas proposed in the current technical literature for the evaluation of the shear capacity of masonry walls reinforced with FRCM. According to [37,38], in fact, the shear capacity of a reinforced panel V_n can be determined as the sum of the capacity of the unreinforced masonry panel V_m and of the contribution of the reinforcement V_f, the latter depending (among other factors as specified in the following of the paper) on the number of FRCM layers.

As it is well known, the effectiveness of this type of interventions is mainly related to the adhesion between the FRCM composite and the substrate, as well as between the cementitious matrix and the mesh. Indeed, adhesion capacity is of paramount importance because it is responsible for the transmission of stresses between the different components of the reinforcement system and is essential to ensure effective distribution of shear stress through the system [39–42].

Generally, when using FRCM reinforcement consisting of a bidirectional mesh, it is a common practice to apply the reinforcement to the entire wall surface [21,25] so that interface stresses are distributed on the entire reinforced area. In so doing, bonding stresses are effectively transmitted between the structure and the reinforcement, and therefore the bearing capacity and shear resistance of the wall is increased. Covering the entire wall surface with a bidirectional mesh also offers the advantage of creating a continuous connection between the reinforcement and the substrate. Furthermore, it allows preventing the formation of localized cracks and detachments, ensuring better overall structural integrity. In addition, the use of a bidirectional mesh allows for an even distribution of fibers, which provides an improved strength and ductility of the structural element. The arrangement of both longitudinal and transversal fibers allows stresses to be distributed more efficiently along the entire reinforced surface. In general, FRCM reinforcements externally bonded to structural masonry elements can significantly increase their shear strength; in any case, appropriate experimental investigations are necessary to have a correct estimation of the effectiveness of the reinforcement.

Also for FRCM-reinforced masonry, an estimate of shear strength can be obtained through the diagonal test [16,20,29,30]. The typical procedure involves the preparation of masonry panels having a proper geometry, representative of a portion of the masonry structure in real buildings. Then, they are reinforced with FRCM composite and subjected to diagonal test.

The manuscript reports and describes the results of an experimental investigation concerning masonry panels made with three different types of mortar (lime mortar, cement mortar and cement-lime mortar), subjected to diagonal tests. The experimental campaign considered both unreinforced and reinforced panels (with FRCM bonded to both the lateral surfaces). The experimental outcomes made it possible to evaluate the relationship between the effectiveness of the considered FRCM reinforcement and the type of masonry on which this is applied. In particular, the influence of the type of mortar (lime, cement-lime or cement) used for the masonry on the shear capacity of the panels (both reinforced and non-reinforced) and on the collapse mechanisms was analysed. Furthermore, the results described in this paper contribute to enriching the experimental database available in the literature on this topic. Finally, the predictive capability of design formulas proposed in the literature for the evaluation of the shear capacity of both unreinforced and reinforced masonry panels is analysed in the manuscript [29,30].

The layout of the paper is the following: Section 2 describes the procedure used to analyse the diagonal test results; the overall experimental investigation is reported in Section 3; the test results are analyzed in Section 4 and compared to the shear capacity predicted by equations taken from the literature; final remarks conclude the paper.

2. Diagonal compression tests: determination of stress-strain curves

The shear strength of unreinforced masonry walls can be evaluated through diagonal compression tests according to either ASTM 519–2010 [8] or RILEM LUMB6 [7] standards; this is, in fact, a commonly employed experimental procedure for evaluating the tensile strength of masonry.

Assuming a linear elastic behaviour of the masonry and a membrane stress state at the centre of the panel, the maximum principal stress can be evaluated as $\sigma_I = 0.5\frac{P}{A_0}$. Supposing that failure occurs when the maximum stress reaches the masonry tensile strength f_t, the latter can be evaluated as [43] $f_t = 0.5\frac{P_{max}}{A_0}$. Then, applying the Turnsek–Cacovic criterion the shear strength τ_0 of the material can be determined as:

$$\tau_{max} = \frac{f_t}{1.5} = \frac{1}{1.5}\left(0.5\frac{P_{max}}{A_0}\right) = 0.33\frac{P_{max}}{A_0}, \tag{1}$$

being P_{max} the maximum load and A_0 the net area of the specimen (including the thickness of the reinforcement if present), equal to:

$$A_0 = \left(\frac{w+h}{2}\right)t, \tag{2}$$

where t, w and h are the thickness, width and height of the panel, respectively. Eq. (1) can also be used to calculate the shear stress at the center of the panel at each load step.

The shear strain at the center of the panel can be determined at each load step using the following relation:

$$\gamma = \varepsilon_T - \varepsilon_C, \tag{3}$$

ε_C and ε_T being the compressive and tensile normal strains respectively, occurring along the diagonal directions of the panel.

The mechanical properties of the masonry (i.e.: initial elastic shear modulus G, equivalent elastic shear strain at maximum stress γ_y) can be determined by substituting the experimental $\gamma-\tau$ curve with an equivalent bilinear diagram underlying the same area as schematized in Fig. 1, so that imposing an energy equality between the actual and the approximated diagrams. To this end, only the initial part of the equilibrium path, up to the maximum shear stress, has been considered [16].

In so doing, the masonry shear modulus G is assumed to be equal to the slope of the first branch of the bilinear diagram.

As it is well known, FRCM reinforcements can considerably increase the mechanical performance of masonry panels, also modifying the

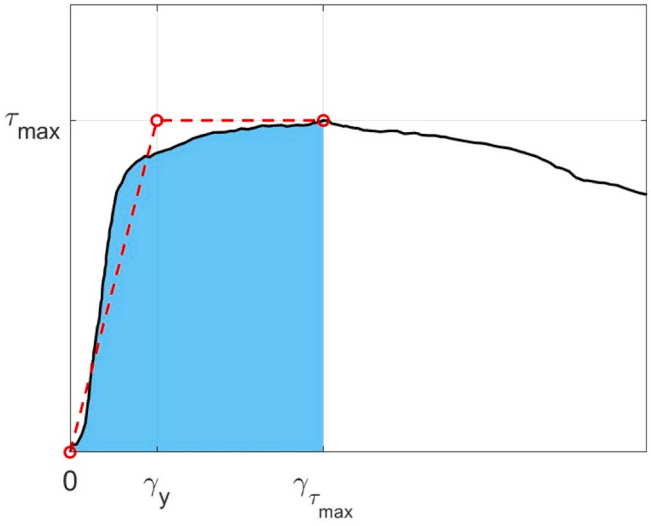

Fig. 1. Representative $\tau-\gamma$ diagram and energy equality to determine the equivalent masonry properties.

collapse mechanisms and increasing the shear strength and generally also the ductility.

Also for masonry panels reinforced with FRCM, the shear behaviour can be experimentally investigated by means of diagonal tests. Their mechanical properties will be assessed in the following sections using Eqs. (1) to (3) and compared to the corresponding parameters estimated for unreinforced masonry [16].

3. Experimental Investigation

The experimental program was aimed at assessing the enhancement in shear behaviour due to the application of a Fiber-Reinforced Cementitious Matrix reinforcement system, externally bonded to various types of masonry panels. Clearly, the effectiveness of the reinforcement is influenced by several factors, such as the mechanical characteristics of masonry, the reinforcing system and its arrangement. Within the experimental program, a FRCM reinforcement system was applied to three different types of masonry specimens, having the same brickwork and differing only in the type of mortar employed (lime, cement-lime, and cement). In addition, the mechanical characteristics of the materials (brick and mortars) composing the masonry were determined through preliminary tests.

3.1. Mechanical properties of the materials

The mechanical properties of the materials considered in the experimental campaign are described in this section. In particular, the properties (experimentally determined) of the materials used to manufacture the masonry panels are described in Section 3.1.1 while the main properties of the materials composing the reinforcement, declared by the manufacturer, are described in Section 3.1.2.

3.1.1. Brick and mortars

The water/cement/lime/sand ratio used to mix the three types of mortars employed in the experimental program is reported in Table 1 [43].

The components of the mortar were mixed using a kneading machine while gradually adding water up to the specified amount. According to EN 1015–11 [44], three specimens having dimensions 160×40×40 mm^3 were produced for each mortar type. After 28 days of curing at room conditions, these were subjected to three-point bending and compression tests.

The compression strength of bricks was determined by carrying out uniaxial compression tests on 6 specimens having size 20×20×40 mm^3, obtained by cutting standard fired-clay bricks. The obtained average values of the mechanical properties for both mortars and bricks are summarized in Table 2 [43].

3.1.2. Fiber Reinforced Cementitious Matrix (FRCM)

A stabilized inorganic mortar matrix (M20, according to the technical datasheet) and a bi-directional PBO mesh (22 g/m^2 in the warp direction and 22 g/m^2 in the weft direction, see Fig. 2) compose the FRCM reinforcing system considered in the experimental program. The main mechanical properties provided by the manufacturer of both the mesh and the matrix are reported in Table 3.

Table 1
Composition of the considered mortar types [43].

Type of mortar	Water/ Cement/ Lime/ Sand (weight ratio)
lime (Ca)	2/-/2/8
cement-lime (MB)	2/1/1/8
cement (Ce)	2/2/-/8

Table 2
Average values of compressive σ_c and flexural σ_f strength [43].

	Brick	Lime Mortar	Cement-lime Mortar	Cement mortar
σ_c (MPa)	17	0.96	2.75	8.33
σ_f (MPa)	/	0.17	0.89	2.63

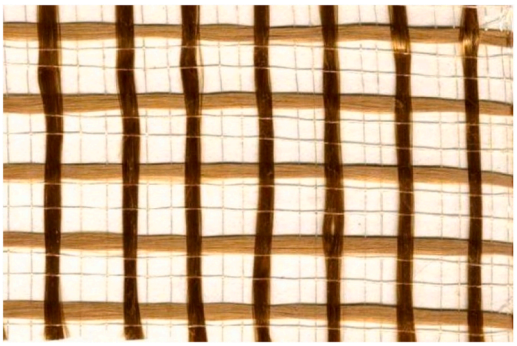

Fig. 2. PBO mesh; 22 g/m^2 in both warp and weft directions.

3.2. Specimens

Eighteen single-leaf masonry panels, 410 × 410 × 49 mm^3 in size, were built and subjected to diagonal compression tests as per [7]. These panels were assembled employing bricks of dimensions 100 × 49 × 21 mm^3, obtained by cutting standard fired-clay bricks, and mortar joints having thickness of about 3 mm. The brickwork was defined to reproduce a typical arrangement of a single leaf masonry (see Fig. 3).

The panels considered in the experimental program were divided into six series of three specimens: three series of three unreinforced specimens and three series of three FRCM-reinforced specimens, varying in the type of matrix in which the textile was embedded. Specimens made with lime, cement-lime and cement mortar are referred to as MCa, MB and MCe in the paper. The reinforcement, composed of a single layer of mesh having warp and weft directions parallel to the masonry joints, was applied to both faces of the specimens, covering the entire area (Fig. 4), as suggested in [44].

As for the labelling of the specimens, MCa, MB and MCe refer respectively to specimens made with lime, cement-lime and cement mortar; FRCM was added for reinforced specimens (see Table 4).

The masonry panels were manufactured on a flat, clean surface. The bricks were properly moistened before being used; particular care was taken to ensure that the mortar layers had uniform thickness and were entirely filled with mortar.

The masonry walls underwent a 28-day curing process within a temperature range of 10 to 30 °C and a relative humidity of 90–100 % [7]. Subsequently, the reinforcement was applied using a wet-lay-up procedure, as outlined in the technical sheet. Specifically, the surface of the panel was brushed, cleaned, and adequately moistened. A preliminary 3 mm thick layer of matrix was then applied, followed by the placement of the mesh. Subsequently, a second 3 mm thick layer of mortar was laid (Fig. 4). To prevent differential shrinkage, cracking, or premature debonding of the reinforcement, the bonded area was covered with wet cloths and a plastic film; moreover, the specimens were encased in plastic bags during the curing phase.

3.3. Test setup

The specimens were positioned inside the testing machine using two steel shoes (Fig. 5), connected through a spherical hinge to the testing machine, to ensure that the load was applied parallel to the vertical diagonal of the specimen. The metal shoes also guaranteed the force to be distributed over a sufficiently large area, avoiding stress

Table 3
Mechanical properties of the reinforcing system components (provided by the manufacturer).

	Equivalent thickness of the mesh	Tensile Young's modulus E_f of the dry mesh	Ultimate tensile strain of the fibre	Toughness	Compressive strength at 28 days	Compressive Young's modulus at 28 days
	[mm]	[GPa]	[%]	[GPa]	[MPa]	[MPa]
PBO fibre	–	270	2.5	5.80	–	–
Bi-directional PBO mesh	0.014	241	–	–	–	–
Inorganic matrix	–	–	–	–	$\geq$ 20	$\geq$ 7500

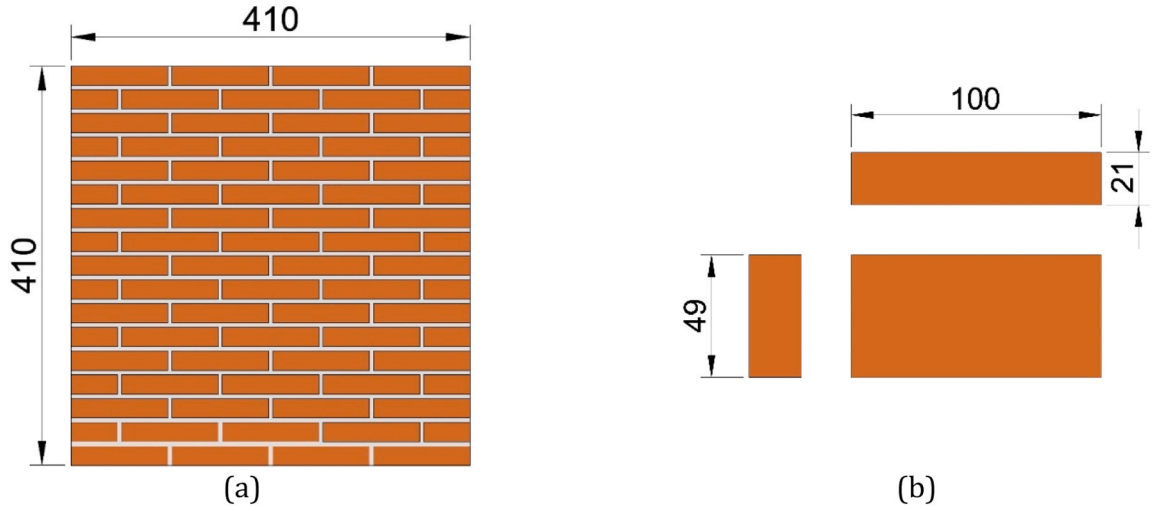

Fig. 3. (a) Geometry of the masonry panels (measures in mm); (b) dimension of the 1:2.5 scaled brick.

concentration and, consequently, local failure at the corners. To assure an optimal contact between the specimen and the steel shoe, a gypsum capping was interposed.

The load, applied by using a screw jack, was measured by a load cell, positioned in series between the loading machine and the upper steel shoe (Fig. 6). During the tests, two displacement transducers measured the vertical displacement of the upper steel shoe. Since the strains generated at the center of the panel were particularly important, accurate measure was provided by applying four omega transducers (gauge length 50 mm) to the center of the specimen along the diagonals of the panel (two on the front face and two on the back face). These instruments, at each loading step, allowed to calculate the compressive ε_C and tensile ε_T axial strains (as the average of the values measured at both faces) and, consequently, the shear strains through Eq. (3).

The tests were carried out by increasing monotonically the vertical displacement of the upper shoe.

4. Experimental results

In this section the main experimental results are described, and the experimental load-displacement diagrams are shown. Then, the failure modes of the specimens are examined and, finally, the shear stress-strain curves, referred to the central part of the panel, are analysed in detail.

This approach allows to analyse the influence of the three types of considered mortar on both the shear behaviour of the unreinforced and reinforced panels and the effectiveness of the strengthening system.

4.1. Load-displacement diagrams

The load-displacement curves obtained from the experimental tests are reported in Fig. 7; Fig. 7a, b and c refer to the unreinforced specimens, while Fig. 7d, e and f refer to the reinforced ones. The average value of displacements measured by the transducers placed at the upper shoe is reported in abscissa and the total applied load is reported in ordinate.

For each series of specimens, average values of the maximum load (F_{max}), the displacement (d_{Fmax}) recorded in correspondence to F_{max} and the ultimate displacement (d_{Fu}), conventionally assumed as that corresponding to a post-peak load equal to 80 % of F_{max}, were calculated. The average and coefficient of variation (CoV) of load values are reported in Table 5, as well as d_{Fu}/d_{Fmax} ratio; the latter can be considered as a first measure of ductility and is used in this paper for comparison purpose.

As shown in Fig. 7a, all the load-displacement diagrams referring to MCa specimens are characterized by three branches: an initial rather linear branch is recorded; then the second one shows a decreasing slope, highlighting the effects of the first damage in the specimen resulting in loss of stiffness; the third final stage highlights a softening behaviour, with progressive damage, leading to the failure of the specimen. Overall, the values of the maximum load (F_{max}) exhibited by the MCa specimens are quite low (average value 4.17 kN in Table 5), due to the low strength of the lime mortar joints. By observing the coefficient of variation of the maximum load equal to 5.59 %, it is worth noting that the global behaviour of the specimens appears to be quite regular in terms of load-bearing capacity. The displacement values $d_{F_{max}}$ and d_{F_u} are very scattered (coefficients of variation of about 40 %); this can be attributed to the shape of the equilibrium path (see Fig. 7a) which presents a sort of plateau near the maximum load for almost all specimens. This could lead, for this series, to some oscillation in the determination of the displacement values reported in the Table 5. Nevertheless, their ratio $d_{F_u}/d_{F_{max}}$, although very low given the brittle behaviour of the specimens, shows a fairly regular trend (coefficient of variation of 8.06 %).

All the load-displacement diagrams of the MB specimens (Fig. 7b) are characterized by two quasi-linear branches: the average slope of the second branch is lower than that one of the first branch due to crack formation and growth in the specimens. At the end of the second branch,

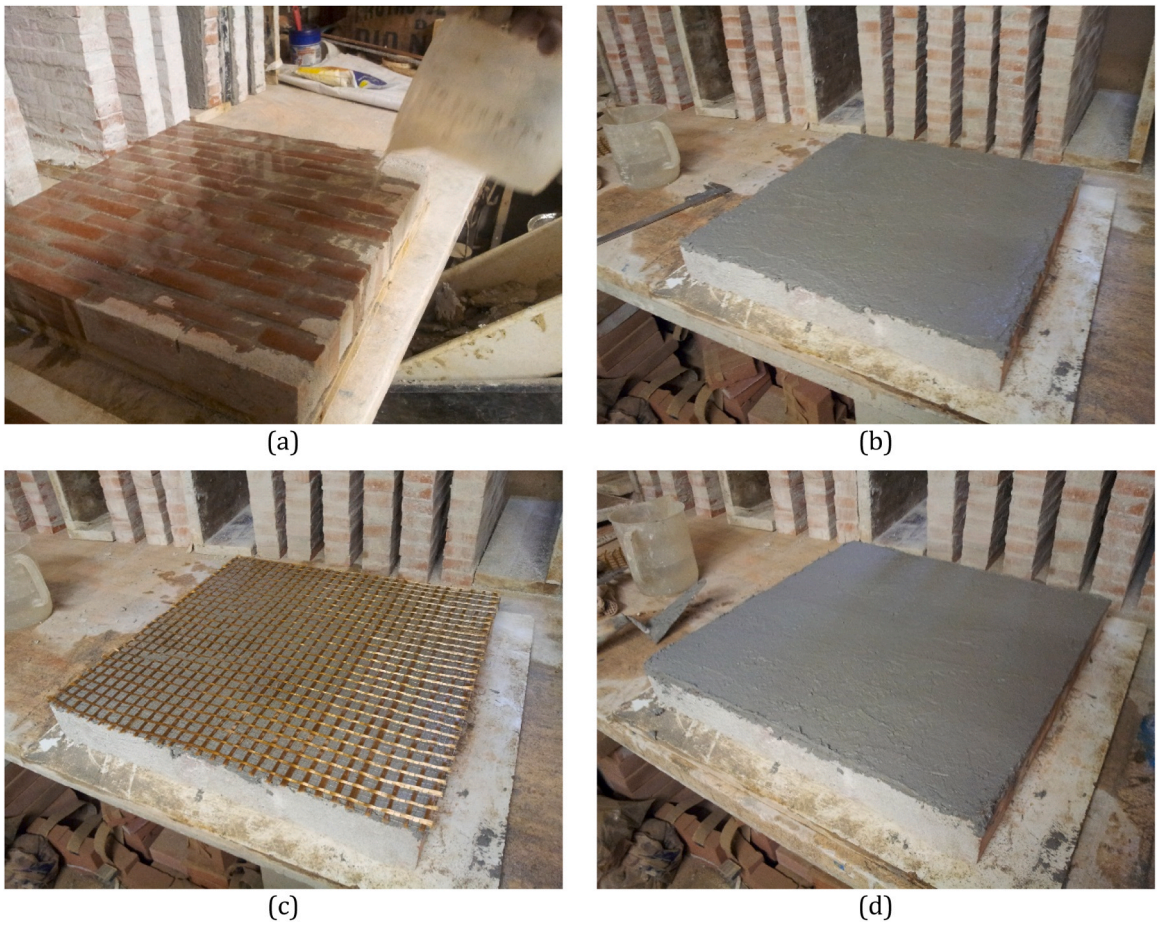

Fig. 4. Specimens' preparation: application of the FRCM reinforcement. (a) Moistening of the surface to be reinforced; (b) application of the first layer of matrix; (c) application of the PBO mesh; (d) application of the second layer of matrix.

Table 4
Characteristics of the specimens considered in the experimental program.

Series	Type of mortar	FRCM reinforcement	Number of specimens
MCa	lime	No	3
MCaFRCM	lime	Yes	3
MB	cement-lime	No	3
MBFRCM	cement-lime	Yes	3
MCe	cement	No	3
MCeFRCM	cement	Yes	3

the load-displacement equilibrium path shows a sharp decrease, corresponding to a brittle failure mode which is highlighted by the low value of the $d_{F_u}/d_{F_{max}}$ ratio (average 1.14, CoV 13.04 %). Therefore, the mechanical properties of the cement-lime mortar, which are higher than those of lime mortar, resulted in a pronounced increase in maximum load of MB specimens (average value 8.47 kN, CoV 2.14 %) with respect to that of MCa specimens, even if the failure mode remained brittle.

Finally, all the load-displacement diagrams of the MCe specimens (Fig. 7c) are characterized by a nearly linear behaviour up to a very brittle failure mode. Nevertheless, the specimens with cement mortar have shown to provide the best response in terms of maximum load ($F_{max} = 31.81kN, CoV = 7.06\%$).

Therefore, experimental results clearly highlight that the type of mortar used to bond the bricks of the specimens strongly affects the behaviour of the panels.

Furthermore, by comparing the load-displacement diagrams of the unreinforced and FRCM-reinforced panels, it is evident that the type of mortar highly influences the effectiveness of the reinforcement as well. The marked improvement in terms of load-bearing capacity is in fact immediately noticeable.

The MCaFRCM specimens (Fig. 7f) show an initial pseudo-linear behaviour, approximately up to the peak load; then a non-uniform post-peak behaviour occurs, very different in the three diagrams. The reason for this different post-peak behaviour and the consequent high CoV values referring to displacements reported in Table 5, can be attributed to the low strength of the lime mortar that causes, in the post-peak phase, the disaggregation of the masonry, generating irregularities on the contact surfaces between masonry and reinforcement, thus reducing its adhesive capacity.

All the specimens exhibited similar values of maximum load (average value 47.36 kN, CoV 9.20 %) and the FRCM reinforcement provided a significant increase in both the load bearing capacity (about +43 kN) and the ductility (about +36 %).

The three diagrams of the MBFRCM specimens (Fig. 7e) show a quite regular behaviour. The reinforcement increased the load bearing capacity of about + 48 kN and the ductility of about + 53 %. From the load displacement curves with a long post-peak softening branch, it is worth noting that the FRCM reinforcement provides MB specimens with a quite ductile behaviour.

A very similar behaviour is observed in the load-displacement diagrams of the MCeFRCM specimens (Fig. 7); the first linear phase is followed by a long softening branch until the occurrence of collapse. Therefore, the increase in the $d_{F_u}/d_{F_{max}}$ ratio of about + 82 % shows that FRCM reinforcement allows a more ductile failure of the MCe specimens by avoiding the typical brittle failure mode observed in the corresponding unreinforced specimens. Finally, the increase in the load bearing capacity produced by the reinforcement was about + 31 kN.

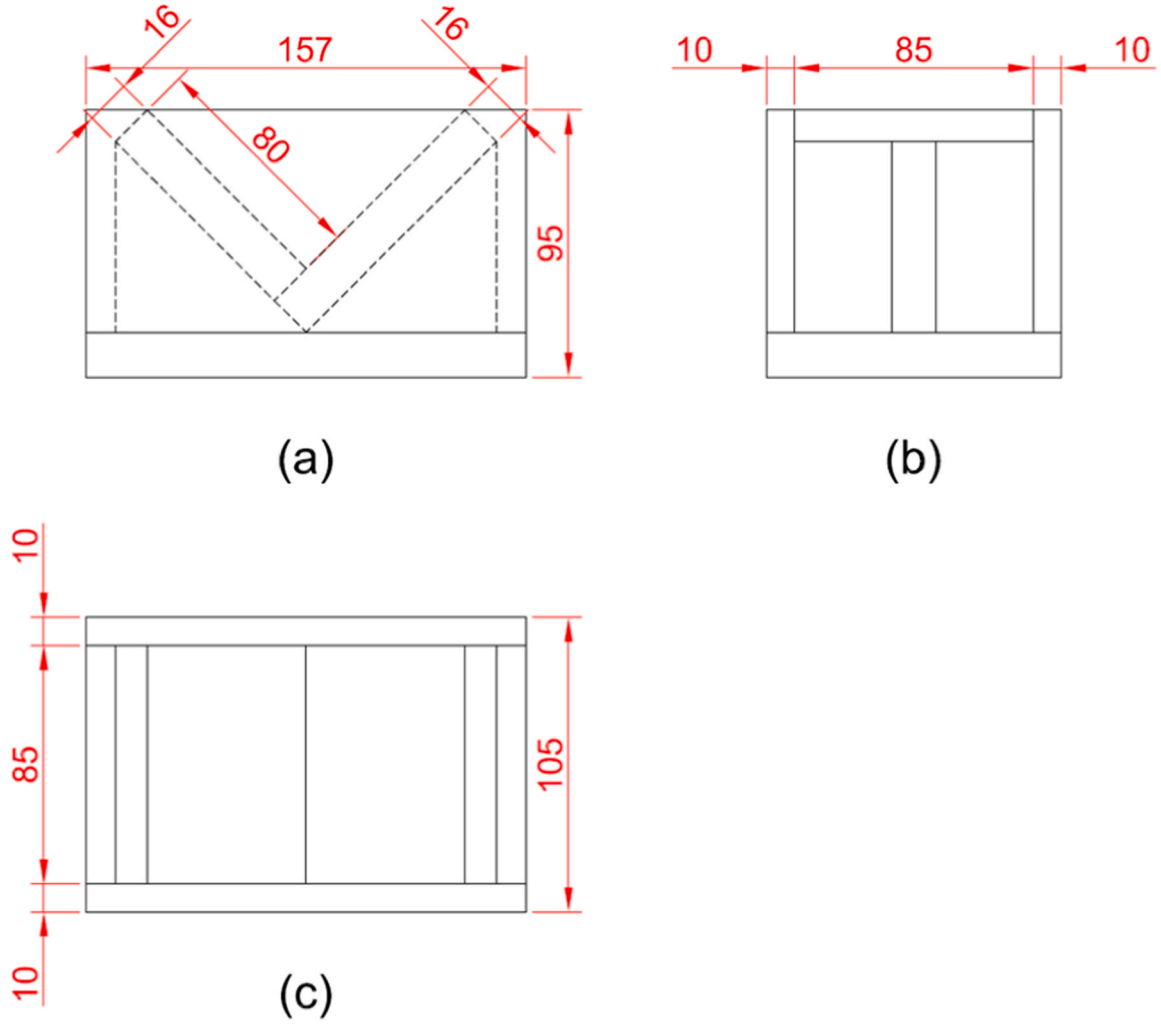

Fig. 5. Geometry of the steel shoe used to apply the load (dimensions in mm): a) front view; b) lateral view; c) plan view.

Note that all these specimens exhibited low scattering in the load bearing capacity, as it is shown by the coefficient of variation which ranged from 2.41 % to 14.65 %.

4.2. Experimental failure modes

The failure modes exhibited by the unreinforced specimens bonded with lime, cement-lime and cement mortars are shown in Fig. 8a,b,c. The failure mode of all three MCa specimens, which are characterized by a very weak mortar, occurred as follows (Fig. 8a): in correspondence to the end of the first quasi-linear branch of the load-displacement diagram a single crack originated approximately at the center of the panel; subsequently, as the load increased this crack propagated roughly in the direction of the vertical diagonal, along the mortar joints (denoted as stepped-stair-mode shear sliding failure in the literature). In the post-peak (softening) phase, the cracks widened and then the specimens failed.

The three MB specimens exhibited a more widespread crack pattern than the MCa specimens but still characterized by cracks following the mortar joint pattern (Fig. 8b). Also in this case, the onset of the main cracks involved the central part of the panel, for a load value at the end of the first linear branch of the load-displacement diagrams; then they propagated almost parallel to the vertical diagonal of the panel (stepped-stair-mode shear sliding failure). For load values in the post-peak branch of the load-displacement diagrams, the cracks widened until the occurrence of the specimen failure.

A rather different behaviour was observed in the MCe specimens (Fig. 8c), due to the higher mechanical properties of the (cement) mortar used to bond the bricks. In fact, starting from the central part of the specimens the cracks followed the vertical diagonal, as in the other specimens, but affected both mortar joints and bricks (diagonal tension failure mode). However, the crack pattern is characterized by a more widened main crack.

The application of reinforcement produced a similar failure mode for specimens of all series, regardless of the mortar used in the masonry (diagonal tension failure mode). In fact, as shown in Fig. 9, initially a series of vertical cracks formed at the centre of the specimen, predominantly arranged according to the compressed diagonal, and subsequently (at the end of the test) the detachment of the reinforcement from the masonry occurred. By comparing the three series of reinforced specimens, it is highlighted that the number of cracks is different and smaller cracks occurred in the less ductile specimens (MCaFRCM, Fig. 9a), while wider cracks occurred in the more ductile ones (MCeFRCM, Fig. 9c).

4.3. Evaluation of $\tau - \gamma$ diagrams

Eq. (1) was used to estimate the shear stress at the centre of the panel at each loading step. To correlate such values to the local values of shear strain γ, the latter was estimated using experimental measurements referred to a small portion of the central part of the panel. Specifically, the shear strain γ was estimated through Eq. (3) using values of

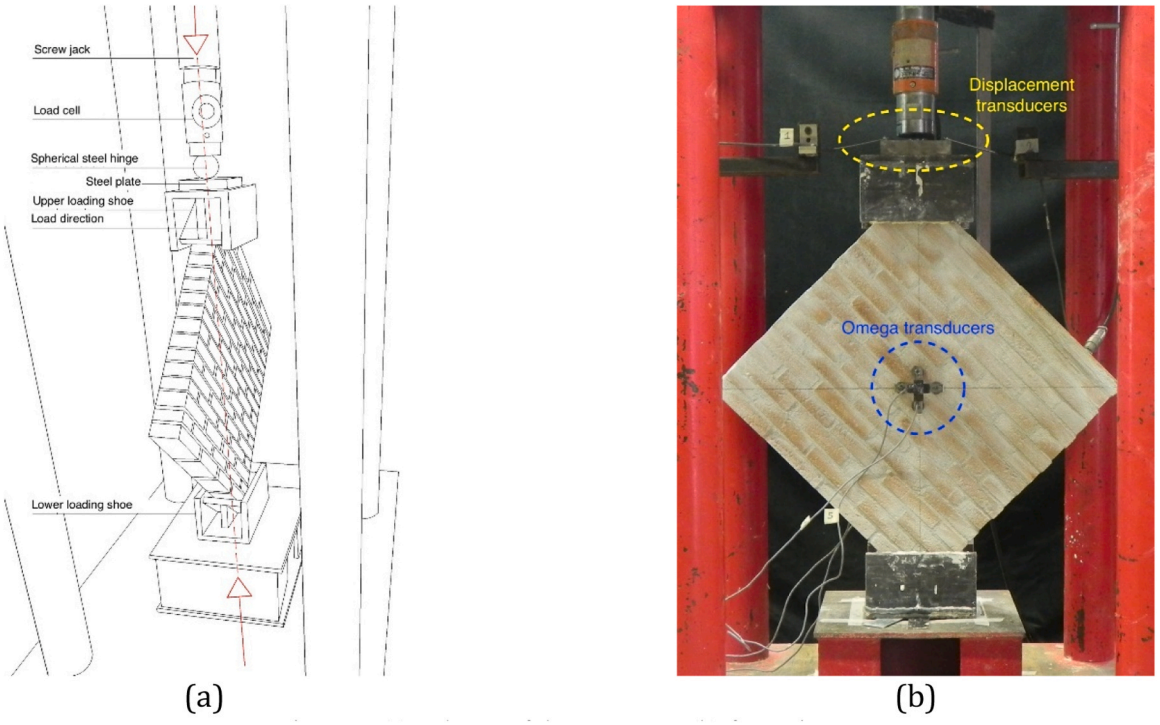

Fig. 6. (a) Scheme of the test setup; (b) front view.

compressive ε_C and tensile ε_T strains obtained through omega transducers positioned at the centre of the panels (Fig. 6), having gauge lengths of 50 mm and such as to intercept only one perpend joint and two bed joints.

The shear stress – shear strain diagram in Fig. 10 show that the specimens of the different series exhibited quite different behaviour from each other. All the diagrams of MCa series show a first nearly linear branch until the occurrence of the first cracks. Thus, almost all the diagrams show a "global" decrease in slope and a softening branch beyond the maximum load. The trend in the diagrams of MCe and MB series is different, since they show a sharp decrease in the shear stress after the maximum load is reached, thus confirming the brittle behaviour.

The average values of the initial shear modulus (G), of the maximum shear strength (τ_{max}) and of the equivalent elastic shear strain at maximum stress (γ_y) are reported in Table 6 as well as the coefficients of variation. It is noted that MCa and MB specimens show quite similar values of G, whilst MCe specimens exhibited higher values, due to the higher mechanical properties of the cement mortar; it is noteworthy that, regardless of the type of mortar used to bond the bricks, all the FRCM reinforcement showed an increase in the initial shear modulus of about 340 MPa; in fact, in the initial part of the tests the composite reinforcements and the masonry panel behave as parallel springs.

Note that γ_y values are very scattered for some specimen's series. These also produce high scattering of the G values given the procedure used to determine this parameter (see Section 2). The high values of CoV could be due to the length of the displacement transducers used in the test setup (see Fig. 9). In fact, during the tests, omega transducers having a gauge length of 50 mm were used in order to have very accurate displacement measurements at the centre of the panel. This choice, however, leads to displacement measurements that are sensitive to the specific crack pattern occurring during the tests; therefore, also the γ_y values, obtained according to Eq. (3), are susceptible to high dispersion.

The trend of the τ_{max} values (refer to Fig. 11 and Table 6) of the unreinforced specimens is in agreement with the mechanical characteristics of the mortars used in the different masonry panels: the MCa specimens showed the lowest values (average value of τ_{max}= 0.069 MPa), the MB specimens showed intermediate values (0.141 MPa) while the MCe specimens showed the highest strength values (0.833 MPa). The reinforced specimens also showed similar trends but, differently from the initial stiffness, reinforcement produced similar strength increases for the MCa and MB specimens ($\Delta\tau_{max}$ of about 0.6 MPa) while smaller increases were observed for the MCe specimens ($\Delta\tau_{max} = 0.3MPa$). It is worth noting that the values of τ_{max} show a very low scattering (similarly to F_{max}).

4.4. Shear capacity: comparisons with design formulas

As commonly proposed in the literature, the shear capacity of reinforced panels V_n can be determined by adding the capacity of the unreinforced masonry V_m and the contribution of the reinforcement V_f [37]. With this approach, the effectiveness of reinforcement is taken into account only after the occurrence of cracks within the masonry wall.

The contribution of masonry V_m depends on the failure mechanism of the unstrengthened masonry wall which is experimentally observed and well known in the literature [23,30,46]. In particular, four failure mechanisms are expected for a wall subjected to diagonal compression and four corresponding in-plane capacities can be computed accordingly; in the following, V_{ss} refers to shear sliding capacity, V_{sf} to shear friction capacity, V_{dt} to diagonal tension capacity and V_c to toe crushing capacity. As a consequence, the shear capacity of the masonry wall is taken as the minimum value, according to Eq. (4) [29,37,46,47]:

$$V_m = \min\left(V_{ss},\quad V_{sf},\quad V_{dt},\quad V_c\right). \tag{4}$$

Capacity in terms of shear sliding, caused by adhesion failure along the bed joints, is computed through the following formula, according to Mohr-Coulomb criterion:

$$V_{ss} = \frac{\tau_0}{1-\mu_0 \tan\theta} A_n, \tag{5}$$

where τ_0 is the adhesion strength of the mortar and is assumed to be equal to 3 % of the masonry compressive strength $f_m^{'}$ [48], μ_0 is the shear friction parameter and is assumed to be equal to 0.3 in [46], $\tan\theta$

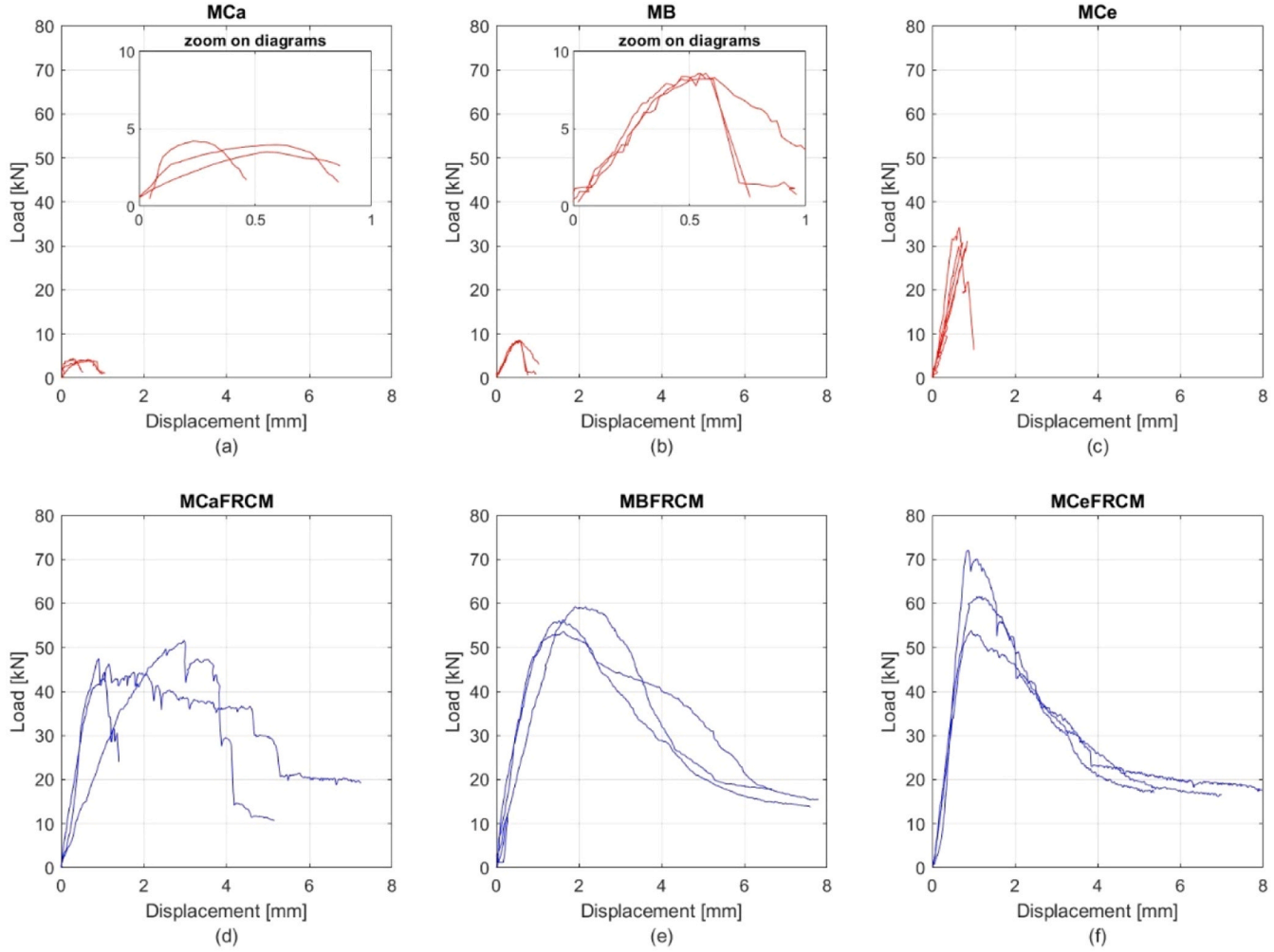

Fig. 7. Experimental load-displacement diagrams of the specimens: (a) MCa and (d) MCaFRCM refer respectively to unreinforced and reinforced specimens made with lime mortar joints; (b) MB and (e) MBFRCM refer to specimens made with cement-lime mortar joints; (c) MCe and (f) MCeFRCM refer to specimens made with cement mortar joints.

Table 5
Average values and coefficient of variation (CoV) of maximum load F_{max}, displacement at maximum load $d_{F_{max}}$ and displacement at ultimate load d_{F_u} (conventionally, $F_u = 0.80F_{max}$).

Series	F_{max}		$d_{F_{max}}$		d_{F_u}		$d_{F_u}/d_{F_{max}}$	
	Mean [kN]	CoV [%]	Mean [mm]	CoV [%]	Mean [mm]	CoV [%]	Mean [–]	CoV [%]
MCa	4.17	5.59	0.57	44.41	0.67	38.77	1.18	8.06
MCaFRCM	47.36	9.20	1.64	70.97	2.39	56.31	1.61	45.74
MB	8.47	2.41	0.56	1.89	0.64	11.13	1.14	13.04
MBFRCM	56.34	4.98	1.68	11.76	2.92	11.03	1.74	3.67
MCe	31.81	7.06	0.72	16.99	0.77	10.01	1.08	6.52
MCeFRCM	62.47	14.65	0.97	10.76	1.91	16.95	1.97	13.70

represents the ratio between the height h and the base w of the panel and A_n is the area of the horizontal cross section of the masonry wall.

Based on the Mohr-Coulomb criterion, the shear capacity related to a stepped-stair failure mode can be calculated, assuming a linear distribution of the normal stress with zero value at the brick center and maximum value at the brick edges, through the following equation [49]:

$$V_{sf} = \frac{\tau_{0,m}}{1 - \mu_m \tan\theta} A_n, \tag{6}$$

where:

$$\tau_{0,m} = \frac{\tau_0}{1 + 1.5\mu_0 \frac{h}{w}} \tag{7}$$

and

$$\mu_m = \frac{\mu_0}{1 + 1.5\mu_0 \frac{h}{w}} \tag{8}$$

h and w being the height and length of the bricks composing the wall, respectively.

Capacity in terms of diagonal tension, a failure which occurs when

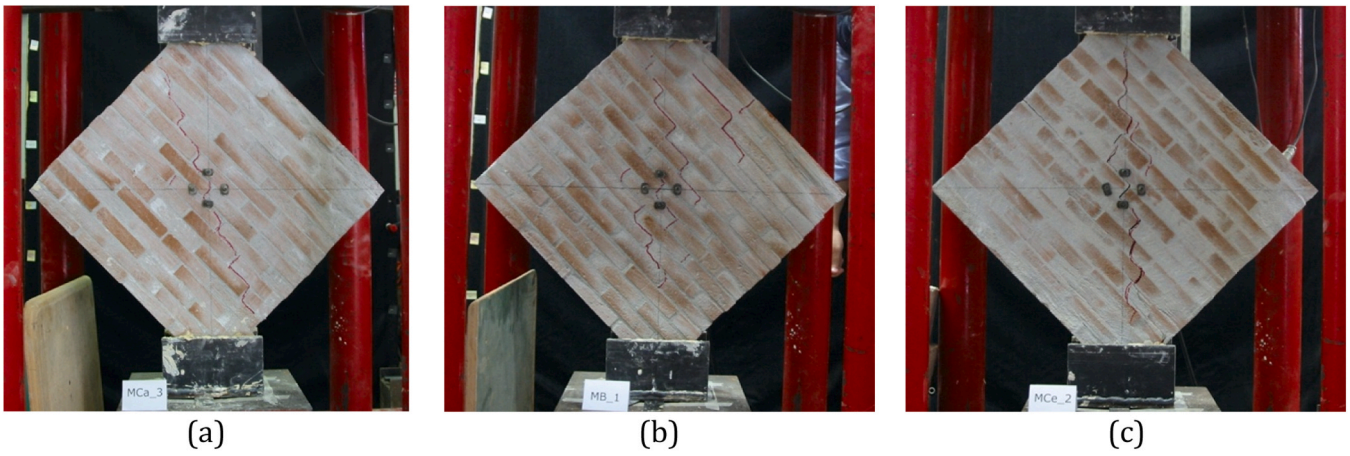

Fig. 8. Failure modes of unreinforced panels; (a) MCa; (b) MB; (c) MCe.

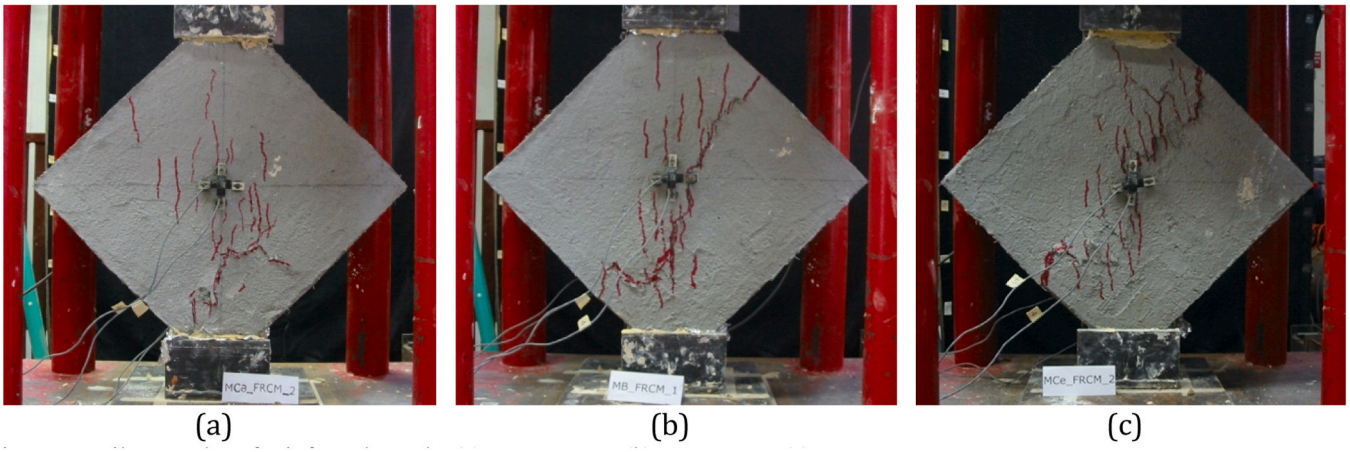

Fig. 9. Failure modes of reinforced panels; (a) MCaFRCM; (b) MBFRCM; (c) MCeFRCM.

the principal tension stress caused by compression forces combined with shearing forces exceeds the tensile strength of the wall, is computed according to the following equation:

$$V_{dt} = \frac{\tan\theta + \sqrt{21.16 + \tan\theta^2}}{10.58} f_t' A_n, \tag{9}$$

where $f_t' = 0.67\sqrt{f_m'}$ is the tensile strength of masonry.

Capacity in terms of toe crushing, caused by the concentration of stress at the loading end that exceeds the compressive strength of masonry [46,47,50], is computed through the following equation:

$$V_c = \frac{2wf_m'}{3h + 2w\tan\theta} A_m, \tag{10}$$

where A_m is the loading area, i.e. the surface between the wall and the steel shoe.

To improve the shear-bearing capacity of masonry walls, FRCMs can be used. The current Italian guideline [38], developed by the Italian National Research Council (CNR), provides a symmetric application of FRCM strengthening on both sides of the wall and extended to the entire surfaces. According to this guideline, the contribution of FRCM reinforcement V_f is provided by the following equation:

$$V_f = \frac{1}{\gamma_{Rd}} n_f t_{vf} l_f \alpha_f \varepsilon_{fd} E_f, \tag{11}$$

where γ_{Rd} is a partial safety factor and it is assumed to be equal to 2 to perform the safety analyses at the ultimate limit state, n_f is the number of FRCM layers, t_{vf} is the equivalent thickness of one layer with fibers aligned along the shearing load direction, l_f is the length of the reinforcement in the direction orthogonal to the shearing load (which cannot exceed the maximum dimension, between length and height, of the wall), α_f is a factor which incorporates the lowering of fiber extensional strength subject to shearing loads and it is given the value 0.80 if experimental results are lacking, E_f is the modulus of axial elasticity of the dry fabric, $\varepsilon_{fd} = \eta \frac{\varepsilon_{fk}}{\gamma_m}$ is the design strain of the FRCM reinforcement and is computed as the ratio between the characteristic value of the FRCM axial strain ε_{fk} and the partial safety factor γ_m assumed equal to 1.5 for Ultimate Limit States, reduced by means of the environmental conversion factor η which depends on indoor ($\eta = 0.90$) or outdoor ($\eta = 0.80$) FRCM applications or applications in aggressive environmental conditions ($\eta = 0.70$). It is worth noting that the product $n_f t_{vf} l_f$ in Eq. (11) describes the equivalent area of the effective shear reinforcement, aligned along the shearing load direction, intersecting a shear crack inclined at 45°.

Eqs. (4) to (11) were used to predict the shear capacity of both the unstrengthened and the FRCM-strengthened wall specimens tested in the laboratory by the authors. Experimental and numerical results are presented in Table 6.

Experimental values reported in the first row of the table are computed as the shearing component of the maximum vertical load applied along the main diagonal of the specimens. Regardless of the failure mode experienced in the experimental tests, all four shear ca-

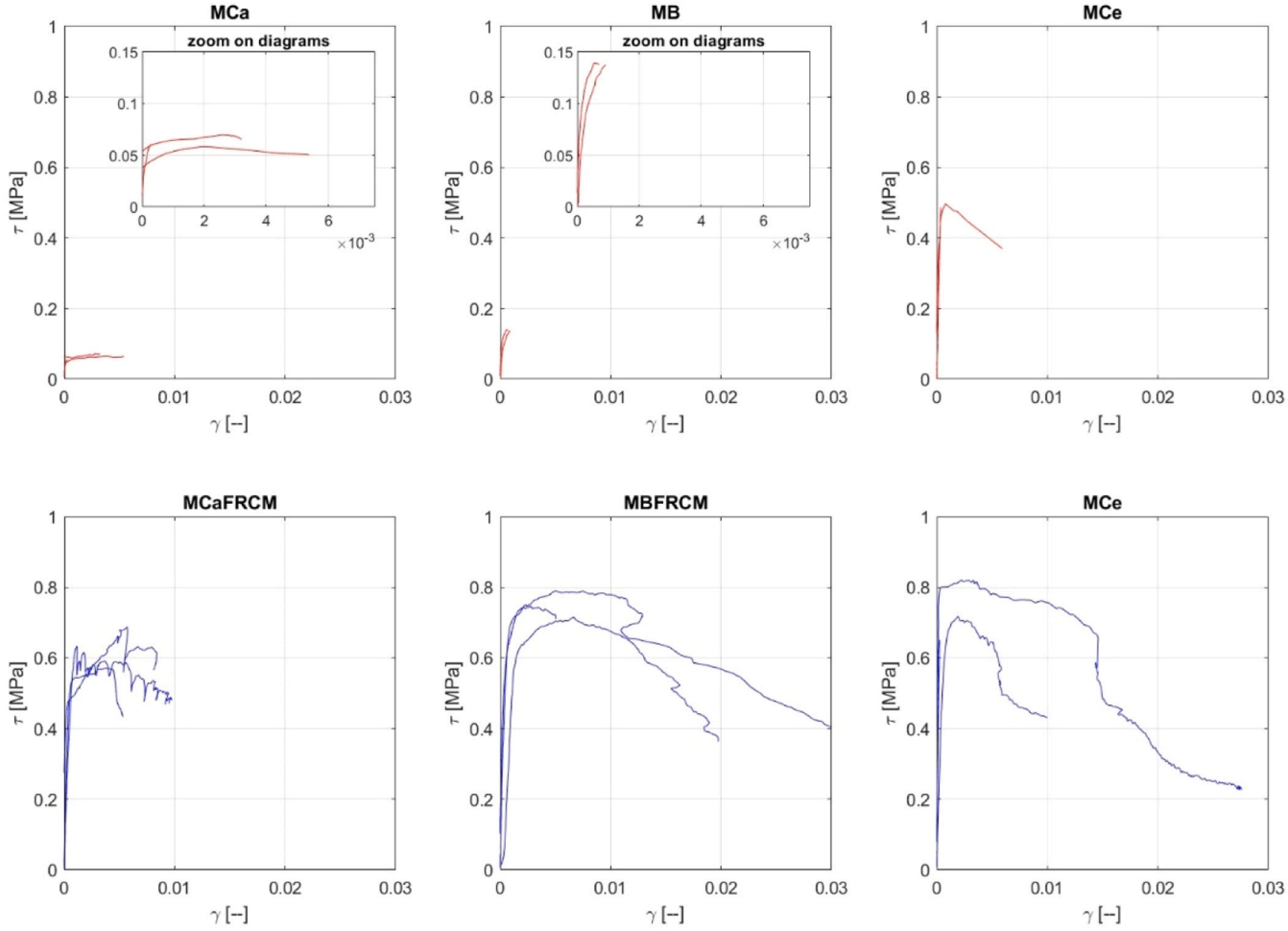

Fig. 10. Shear stress-shear strain diagrams obtained from the experimental data: MCa and MCaFRCM refer respectively to unreinforced and reinforced specimens made with lime mortar joints; MB and MBFRCM refer to specimens made with cement-lime mortar joints; MCe and MCeFRCM refer to specimens made with cement mortar joints.

Table 6
Average values and coefficient of variation (CoV) of the shear strength τ_{max}, equivalent elastic shear strain γ_y at maximum stress, initial elastic shear modulus G.

Series	τ_{max}		γ_y		G	
	Mean [MPa]	CoV [%]	Mean [μ]	CoV [%]	Mean [MPa]	CoV [%]
MCa	0.069	5.59	137.57	–	504.01	–
MCaFRCM	0.631	9.20	714.09	7.79	844.36	0.56
MB	0.141	2.41	253.57	–	561.54	–
MBFRCM	0.751	4.98	905.80	34.81	897.28	31.12
MCe	0.528	7.06	286.69	29.65	1842.10	27.04
MCeFRCM	0.833	14.65	539.13	68.57	2176.61	83.22

pacities of the unstrengthened masonry wall specimens were calculated and it is worth noting that the predictions that best match the experimental results are obtained by using the equation of the shear friction capacity V_{sf} (Eq. (6)) for MCa and MB specimens which, indeed, experienced a shear friction failure mode, and the equation of the diagonal tension capacity V_{dt} (Eq. (9)) for MCe specimens, which experienced a diagonal tension failure mode in the diagonal compression test.

In the last three columns of Table 6, numerical predictions of the FRCM-reinforced masonry wall specimens are listed. The contribution of the FRCM reinforcement was assessed by using Eq. (11), where γ_{Rd} was assumed equal to 1 for direct comparison with the experimental results. Also in this case, the predictions that best match the experimental results are obtained by using the equation of the diagonal tension capacity V_{dt} (Eq. 9) for all FRCM-reinforced wall specimens, which experienced a

Table 7
Experimental vs. numerical predictions of unstrengthened and FRCM-strengthened wall specimens.

Shearing capacity	Unstrengthened masonry walls			FRCM-strengthened masonry walls		
	MCa	MB	MCe	MCaFRCM	MBFRCM	MCeFRCM
	[kN]	[kN]	[kN]	[kN]	[kN]	[kN]
Experimental	2.95	5.99	22.49	33.49	39.84	44.17
V_{ss}	3.87	7.15	9.47	21.62	24.89	27.21
V_{sf}	3.41	6.30	8.34	21.16	24.04	26.09
V_{dt}	15.40	20.92	24.08	33.15	38.66	41.83
V_c	18.97	34.99	46.37	36.71	52.73	64.11

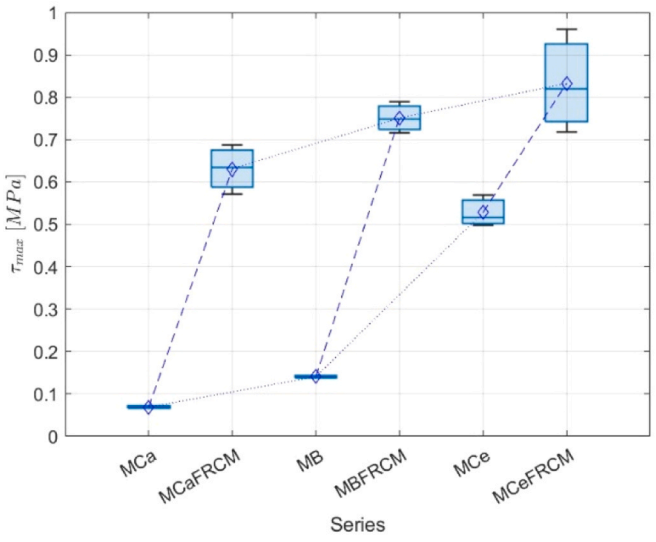

Fig. 11. Box chart diagram referring to the shear strength. The central mark indicates the median, the bottom and top edges of the box indicate the 25th and 75th percentiles, respectively. The whiskers extend to the most extreme data points not considering outliers. The mean values within each series are plotted using the "◊" symbol [45].

diagonal tension failure mode during the test.

Finally, it is noted that the predictions of the shear capacity of FRCM-strengthened walls are conservative values and, therefore, the equation provided by the Italian CNR can be used to safely design the strengthening system.

5. Conclusions

This paper presents the results of an experimental campaign aimed at estimating the shear capacity of masonry panels, both unreinforced and reinforced with externally bonded FRCM, and evaluating the effectiveness of this type of reinforcement applied to three different types of masonry, differing for the type of mortar employed. For this purpose, diagonal compression tests were considered in the experimental campaign.

In line with current trends in the literature, the shear strength of the masonry has been determined according to the Turnsek–Cacovic criterion; this approach was extended to evaluate the equivalent shear strength of the reinforced panels. The diagonal tests also allowed to determine the shear modulus of the masonry and the failure modes of the specimens. Finally, the experimental shear capacity of the panels was compared with the predictions of design formulas proposed in the literature.

Experimental results showed that FRCM reinforcement substantially modified the failure mechanism of the panels by producing, for all three types of masonry considered, thinner and more distributed cracks than for the unreinforced specimens for which, on the contrary, sharper and more localized cracks were developed. Moreover, the reinforcement increased the maximum diagonal load of about 43 kN and 48 kN for specimens with lime and lime-cement mortar joints, respectively. Lower absolute increments (about 31 kN) were recorded for specimens with cement mortar. Quite scattered values of both shear modulus and ductility were obtained from the tests.

Finally, the experimental outcomes have been used to validate the predictive capability of selected literature design formulas. It is worth noting that the formulas proposed to assess the shear capacity of unreinforced masonry panels available in the literature that best fit the experimental outcomes are those corresponding to the failure mode that occurred during the tests. Therefore, if the contribution of the reinforcement is evaluated using the formula corresponding to the actual failure mode, the CNR formula provides quite accurate predictions of the shear capacity of FRCM-reinforced masonry panels.

Declaration of Competing Interest

The authors declare that they have no known competing financial interests or personal relationships that could have appeared to influence the work reported in this paper.

Data availability

Data will be made available on request.

References

[1] Calderini C, Cattari S, Lagomarsino S. In-plane strength of unreinforced masonry piers. Earthq Eng Struct Dyn 2009;38:243–67. https://doi.org/10.1002/eqe.
[2] Satta M L, Ruggieri N, Tempesta G, Galassi S. Remains of the ancient colonnade in the archaeological site of Pompeii, Italy: vulnerability analysis and strengthening proposal. J Cult Herit 2021;52:93–106. https://doi.org/10.1016/j.culher.2021.09.006.
[3] Galassi S, Satta M. L, Ruggieri N, Tempesta G. In-plane and out-of-plane seismic vulnerability assessment of an ancient colonnade in the archaeological site of Pompeii (Italy), Procedia Structural Integrity 2020; 29: 126–133, International Conference Art Collections 2020, Safety Issue (ARCO 2020, SAFETY), 21-23 September 2020. https://doi.org/10.1016/j.prostr.2020.11.148.
[4] Ministero delle Infrastrutture e dei Trasporti. Aggiornamento delle "Norme tecniche per le costruzioni" 2018:1–198.
[5] EC6. Eurocode 6 - Design of masonry structures 1996;1.
[6] EN 1052–3. EN 1052–3 Methods of test for masonry-Part 3: Determination of initial shear strength 2002.
[7] RILEM TC 76-LUM. LUM B6: Diagonal tensile strength tests of small wall specimens. RILEM, Recommendations for the Testing and Use of Constructions. Mater, EFN SPON, Lond, UK 1994:488–9.
[8] ASTM E519/E519M − 10 . Standard Test Method for Diagonal Tension (Shear) in Masonry Assemblages. American Society for Testing Materials 2010:5. https://doi.org/10.1520/E0519 _E0519M-10.
[9] Calderini C, Cattari S, Lagomarsino S. The use of the diagonal compression test to identify the shear mechanical parameters of masonry. Constr Build Mater 2010;24:677–85. https://doi.org/10.1016/j.conbuildmat.2009.11.001.
[10] Chiostrini S, Galano L, Vignoli A. On the determination of strength of ancient masonry walls via experimental tests. Proc Twelfth World Conf Earthq Eng 2000.
[11] Corradi M, Borri A, Vignoli A. Experimental study on the determination of strength of masonry walls. Constr Build Mater 2003;17:325–37. https://doi.org/10.1016/S0950-0618(03)00007-2.
[12] Brignola A, Frumento S, Lagomarsino S, Podestá S. Identification of shear parameters of masonry panels through the in-situ diagonal compression test. Int J Archit Herit 2009;3:52–73. https://doi.org/10.1080/15583050802138634.
[13] Turnesec V, Cacovic F. Some experimental results on the strength of brick masonry walls. Proc. of the 2nd international brick masonry conference. Stoke-on-Trent. British Ceramic Research Association,; 1971. p. 149–56.
[14] Casacci S, Gentilini C, Di Tommaso A, Oliveira DV. Shear strengthening of masonry wallettes resorting to structural repointing and FRCM composites. Constr Build Mater 2019;206:19–34. https://doi.org/10.1016/j.conbuildmat.2019.02.044.
[15] Papanicolaou CG, Triantafillou TC, Karlos K, Papathanasiou M. Textile-reinforced mortar (TRM) versus FRP as strengthening material of URM walls: In-plane cyclic loading. Mater Struct/Mater Et Constr 2007;40:1081–97. https://doi.org/10.1617/S11527-006-9207-8.
[16] Castori G, Corradi M, Sperazini E. Full size testing and detailed micro-modeling of the in-plane behavior of FRCM–reinforced masonry. Constr Build Mater 2021;299:124276. https://doi.org/10.1016/J.CONBUILDMAT.2021.124276.
[17] Shing PB, Schuller M, Hoskere VS. In-plane resistance of reinforced masonry shear walls 1990;116:619–40.
[18] Garbin E., Valluzzi M.R., Modena C., Oliveira D.V., Lourenço P.B. Experimental investigation on the structural behaviour and strengthening of threeleaf stone masonry walls. Proceedings of Structural Analysis of Historical Constructions – SAHC, New Delhi: 2006.
[19] Corradi M, Borri A, Vignoli A. Experimental evaluation of in-plane shear behaviour of masonry walls retrofitted using conventional and innovative methods. Mason Int 2008;21.
[20] Ferretti F, Mazzotti C. FRCM/SRG strengthened masonry in diagonal compression: experimental results and analytical approach proposal. Constr Build Mater 2021;283:122766. https://doi.org/10.1016/j.conbuildmat.2021.122766.
[21] Meriggi P, De Santis S, Fares S, de Felice G. Design of the shear strengthening of masonry walls with fabric reinforced cementitious matrix. Constr Build Mater 2021;279:122452. https://doi.org/10.1016/j.conbuildmat.2021.122452.
[22] Mezrea PE, Ispir M, Balci IA, Bal IE, Ilki A. Diagonal tensile tests on historical brick masonry wallets strengthened with fabric reinforced cementitious mortar. Structures 2021;33:935–46. https://doi.org/10.1016/j.istruc.2021.04.076.
[23] Babaeidarabad S, Arboleda D, Loreto G, Nanni A. Shear strengthening of unreinforced concrete masonry walls with fabric-reinforced-cementitious-matrix.

Constr Build Mater 2014;65:243–53. https://doi.org/10.1016/J.CONBUILDMAT.2014.04.116.
[24] Faella C, Martinelli E, Nigro E, Paciello S. Shear capacity of masonry walls externally strengthened by a cement-based composite material: An experimental campaign. Constr Build Mater 2010;24:84–93. https://doi.org/10.1016/J.CONBUILDMAT.2009.08.019.
[25] Marcari G, Basili M, Vestroni F. Experimental investigation of tuff masonry panels reinforced with surface bonded basalt textile-reinforced mortar. Compos B Eng 2017;108:131–42. https://doi.org/10.1016/J.COMPOSITESB.2016.09.094.
[26] Mazzotti C, Ferretti F, Ferracuti B, Incerti A. Diagonal compression tests on masonry panels strengthened by FRP and FRCM. Struct Anal Hist Constr: Anamn, Diagn, Ther, Controls - Proc 10th Int Conf Struct Anal Hist Constr, SAHC 2016; 2016:1069–76. https://doi.org/10.1201/9781315616995-144.
[27] Parisi F, Iovinella I, Balsamo A, Augenti N, Prota A. In-plane behaviour of tuff masonry strengthened with inorganic matrix-grid composites. Compos B Eng 2013; 45:1657–66. https://doi.org/10.1016/j.compositesb.2012.09.068.
[28] Prota A, Marcari G, Fabbrocino G, Manfredi G, Aldea C. Experimental in-plane behavior of tuff masonry strengthened with cementitious matrix–grid composites. J Compos Constr 2006;10:223–33. https://doi.org/10.1061/(ASCE)1090-0268(2006)10:3(223).
[29] Babaeidarabad S, De Caso F, Nanni A, Asce F. URM Walls Strengthened with Fabric-Reinforced Cementitious Matrix Composite Subjected to Diagonal Compression. J Compos Constr 2014;18:1–9. https://doi.org/10.1061/(asce)cc.1943-5614.0000441.
[30] Sagar SL, Singhal V, Rai DC, Gudur P. Diagonal Shear and Out-of-Plane Flexural Strength of Fabric-Reinforced Cementitious Matrix–Strengthened Masonry Walletes. J Compos Constr 2017;21:1–13. https://doi.org/10.1061/(asce)cc.1943-5614.0000796.
[31] Zampieri P, Santinon D, Pellegrino C, Iodice F, Vecchi A. Effect of Spike Anchors in the Bond Behavior of FRCM Systems Applied onto Curved Masonry Substrates. J Compos Constr 2023;27:4023061. https://doi.org/10.1061/JCCOF2.CCENG-4199.
[32] Alecci V, Ayala AG, De Stefano M, Marra AM, Nudo R, Stipo G. Influence of the masonry wall thickness on the outcomes of double flat-jack test: Experimental and numerical investigation. Constr Build Mater 2021;285:122912. https://doi.org/10.1016/J.CONBUILDMAT.2021.122912.
[33] Zampieri P, Piazzon R, Pantò B, Pellegrino C. A discrete-macro-element-model for the in-plane analysis of masonry structures strengthened by FRCMs. 2021-June COMPDYN Proc 2021:309–17. https://doi.org/10.7712/120121.8484.19046.
[34] Como M, Coccia S, di Carlo F. Plastic Analysis of Masonry Arches Reinforced with FRCM under Vertical and Horizontal Forces. Key Eng Mater 2019;817:236–43. https://doi.org/10.4028/www.scientific.net/KEM.817.236.
[35] Alecci V, De Stefano M, Luciano R, Marra A M, Stipo G. Numerical Investigation on the Use of Flat-Jack Test for Detecting Masonry Deformability. J. Test. Eval. 2020; 49:537–49. https://doi.org/10.1520/JTE20190781.
[36] ACI Committee 549.6R-20. Guide to Design and Construction of Externally Bonded Fabric-Reinforced Cementitious Matrix (FRCM) and Steel-Reinforced Grout (SRG) Systems for Repair and Strengthening Masonry Structures Inch-Pound Units 2020.
[37] ACI Committee 549.4R-13. Guide to Design and Construction of Externally Bonded Fabric-Reinforced Cementitous Matrix (FRCM) Systems for Repair and Strengthening Concrete Structures. 2013.
[38] Consiglio Nazionale delle Ricerche. CNR-DT 215/2018 Istruzioni per la Progettazione, l'Esecuzione ed il Controllo di Interventi di Consolidamento Statico mediante l'utilizzo di Compositi Fibrorinforzati a Matrice Inorganica. CNR: Consiglio Nazionale Delle Ricerche 2018.
[39] Rotunno T, Fagone M, Grande E, Milani G. FRCM-to-masonry bonding behaviour in the case of curved surfaces: experimental investigation. Compos Struct 2023: 116913. https://doi.org/10.1016/j.compstruct.2023.116913.
[40] Bertolesi E, Fagone M, Grande E, Milani G, Rotunno T. Innovative Fiber Optic Sensor monitoring of delamination phenomenon for FRCM reinforced curved masonry pillars. IEEE Int Workshop Metrol Living Environ (MetroLivEn) 2022 2022:144–8. https://doi.org/10.1109/METROLIVENV54405.2022.9826951.
[41] Bellini A, Aiello MA, Bencardino F, de Carvalho Bello CB, Castori G, Cecchi A, et al. Influence of different set-up parameters on the bond behavior of FRCM composites. Constr Build Mater 2021;308:124964. https://doi.org/10.1016/j.conbuildmat.2021.124964.
[42] Grande E, Fagone M, Rotunno T, Milani G. Modeling of shear-lap tests of flat and curved masonry specimens strengthened by FRCM. Structures 2023;52:437–48. https://doi.org/10.1016/j.istruc.2023.04.014.
[43] Alecci V, Fagone M, Rotunno T, De Stefano M. Shear strength of brick masonry walls assembled with different types of mortar. Constr Build Mater 2013;40: 1038–45. https://doi.org/10.1016/j.conbuildmat.2012.11.107.
[44] UNI EN 1015–11. Methods of test for mortar for masonry Part 11: Determination of flexural and compressive strength of hardened mortar 2007;UNI EN 101.
[45] MathWorks. Matlab 9.4.0 2018.
[46] Li T, Galati N, Tumialan JG, Nanni A. Analysis of unreinforced masonry concrete walls strengthened with glass fiber reinforced polymer bars. Acids Struct J 2005; 102:569–77.
[47] Silva PF, Yu P, Nanni A. Monte Carlo simulation for validating the in-plane shear capacity of URM walls strengthened with GFRP grid reinforced polyurea. J Compos Constr 2008;12:405–15.
[48] Paulay T, Priestley MJN. Seismic Design of Reinforced Concrete and Masonry Buildings. New York: Wiley; 1992.
[49] Crisafulli FJ, Carr AJ, Park R. Shear strength of unreinforced masonry panels. Proceedings of the Pacific Conference on Earthquake Engineering. New Zeland: New Zealand National Society for Earthquake Engineering; 1995.
[50] Petersen R. In-plane shear behavior of unreinforced masonry panels strengthened with fiber reinforced polymer strips. University of Newcastle; 2009.